University of Bath

Effect of elastic wheel on urban railway system with wheel-rail coupling vibration model

J.H. Tian[a,b], X.X. Lu[a], G.L.Ma[a], C.R.Bowen[b]

[a]CAE engineering application analysis room, School of Mechatronic Engineering, Xi`an Technological University, Xi'an 710021, China

[b]Department of Mechanical Engineering, University of Bath, Bath A2 7AY, UK

Abstract

This study investigates the wheel-rail coupling vibration（WRCV）of an urban railway system. A combined elastic wheel damping structure is proposed, with the assumption that there is large elastic deformation that leads to a reduction in the vibration of the railway system. We develop a dynamic model of the railway vehicle with an elastic wheel damping structure, which is calculated by the Newmark-β method in the time domain. The effect of stiffness coefficient of elastic wheel on vehicle system motion is studied in detail as the wheel moves on an irregular track. Our results show that the range of vertical acceleration changes with a V-shaped trend with an increase of the stiffness coefficient of the elastic wheel, and the optimum stiffness coefficient of elastic wheel is obtained, where there is a minimum in vertical acceleration. We observe that the peak wheel vibration is more easily affected by the track irregularity when the stiffness coefficient of elastic wheel is small. When attempting to suppress wheel vibration, as the degree of track irregularity becomes smaller, an elastic

wheel with a larger stiffness coefficient is needed. This paper therefore provides new insights on the effect of wheel elasticity on vibration characteristics.

Keywords

Elastic wheel, Wheel-rail, coupling vibration, Track irregularity, Stiffness coefficient

1 Introduction

With the rapid development of the urban railway industry, the noise and random vibration of urban railway system is growing, which reduces the comfort of passengers significantly, and the instability of the railway system increases. The most common method to limit noise and vibrations is to change the elastic structure of the bogie, which is a method for the process of a random impact transfer path. However, due to the complex structure of the bogie, there is an increase in costs to undertake maintenance and overhaul, and a change in bogie parameters can significantly affect the running performance of the whole vehicle system. The emergence of elastic wheels damping structure is an effective method to resolve above-mentioned problem[1]. This is an optimization challenge in terms of the source of the random impact and the relatively simple structure of the wheel provides ample room for improvement. Due to the convenience of disassembly of the wheel, there is a decrease in disassembly and installation time, and maintenance costs are reduced. The use

of an elastic damping structure can also reduce the overall mass of the vehicle and the static load during wheel-rail contact. In particular, the damping structure based on an elastic wheel absorbs the wheel-rail load and reduces the fluctuation amplitude of the wheel-rail interaction. Despite these advantages, there has been little effort to standardize the approach to determine parameters of elastic wheel, which limits its potential application. In addition, the existence of track irregularity represents a source of wheel-rail coupling vibration (WRCV), where the wheel-rail impact is transferred from the wheel to the bogie and finally to the carriage. Since the wheel is the first system to bear the excitation load of track irregularity, it is necessary to understand in more detail the influence of the elastic parameters of the wheel system and track irregularity to reduce the impact load of the wheel-rail system and the random vibrations of wheel. Such new insights are advantageous for the development of future urban railway systems and adoption of new standards for elastic wheels.

Until now, in order to accurately study WRCV and the dynamic characteristics of railway system, scholars have established complex nonlinear models with multiple degrees of freedom. Meysam, Jabbar et al. established a three-dimensional dynamic model of rail vehicle and obtained the wheel-rail force under irregular track. In addition, the vibration characteristics of a wheelset has been researched when both the left and right tracks are irregular[2]. Wenbo, Linchang et al. studied the influence of track parameters on vehicle body vibration[3]. A coupled dynamic model of vehicle-

track-soil was developed, and the influence of damping and stiffness coefficients of each fastening component on vibration of railway system was studied. However, the important influence of wheel on railway system was ignored. Amin established a coupling dynamics model of vehicle-track-soil with a short-wave irregularity of track, and studied the influence of stiffness, speed and harmonic unevenness of the track cushion on wheel-rail force[4]. However, the impact of the elastic wheel damping structure on the vibration of the railway system has yet to be considered. Zefeng Wen, Lei Wu et al. proposed a finite element model with the implementation of an advanced cyclic plasticity theory[5], which was used to study the three-dimensional elastic-plastic rolling contact stresses of wheel and rail. Xin Zhao, Zili Li et al. solved wheel-rail frictional rolling contact using linear elasticity and statics with a half space assumption in three dimensions[6]. Santamaría J, Vadillo EG et al. descrbied a new method to solve the wheel-rail contact problem via a look-up table with a three-dimensional elastic model[7]. In the work above [5-7], the elastic deformation of the wheel was considered, and the elastic contact model and calculation method were proposed. However its elastic deformation was based on a traditional rigid wheel, wheew the elastic deformation is relatively small, and it influence on the vibration of the railway system is not obvious. Based on the models of wheel-rail elastic contact in the aforementioned work, a combined elastic wheel damping structure is proposed in this paper, where the elastic damping structure is added between the wheel center and wheel hub, with the existence of a large elastic deformation, where the vibration

characteristics of the railway system can be reduced effectively. In particular, the relationship between the parameters of elastic components and body dynamics has been studied in detail.

Based on the traditional wheel-rail coupling model of vehicle dynamics, the rigid wheel is replaced with an elastic wheel, and a new wheel-rail coupling model of railway dynamics using an elastic wheel is constructed in this study. The effects of track irregularity and elastic layer stiffness on wheel vibration characteristics are studied using our new dynamic model. The complete vehicle WRCV dynamics model is established with elastic wheels, and wheel-rail force characteristics are determined. Subsequently, elastic parameters and track irregularity are examined as independent variables, where Newmark-β method is used to solve the matrix iteratively in MATLAB. The time course curve of wheel vertical vibration is obtained and the relationship between the vertical vibration of wheel, track irregularity and elastic layer stiffness is studied.

In this paper, a combined elastic wheel damping structure is proposed in order to reduce wheel-rail impact and the vibration of the whole vehicle system, which is composed by wheel hub, elastic damping module and wheel center, with the large elastic deformation. The wheel-rail force is transmitted from the track to wheel hub, elastic damping module, wheel center, and the axle. Due to the existence of an elastic damping module, the wheel-rail impact and vibration of the vehicle system are reduced. Then according to the concept of dynamic balance and D'Alembert's principle, the mass, damping and stiffness matrix of elastic wheel damping structure are designed, and the

vehicle dynamic motion equations are established. Finally, the influence of elastic damping module on wheel vibration is studied through the Newmark-β method in time domain integral, and the optimal stiffness coefficient of elastic damping module is obtained.

2 Establishment of dynamic model

2.1 Dynamic model

In this model, a complete wheel-rail coupling dynamics model with 25 degrees of freedom is established. The model includes one body, two bogies, four pairs of wheels, and eight elastic layers of wheels. According to the principle model shown in the Figure 1, there are three motions: rotation in the X direction(R_x), displacement in the Y direction (Y) and rotation in the Z direction(R_z). The vertical action of the wheel and rail is primarily studied, and the interaction between the side of the track and the wheel affects the lateral movement of the railway system mainly, which is ignored in order to simplify the coupling process[8]. The carriage and bogie have three degrees of freedom of R_x , Y , R_z and each wheelset has two degrees of freedom of R_x , Y . Each elastic wheel hub has one degree of freedom of Y . Since the deformation of the body, bogie and wheelset is small, they are considered as rigid bodies and their elastic deformation is ignored[8]. Each wheelset has two wheels, and each wheel has an elastic layer. The elasticity of the wheel is realized by a linear idealized spring (K_s) and a linear idealized viscous damper (C_s) between the wheel center and the wheel hub. The

body and the two-stage suspension bogie are connected by two sets of K_s and C_s. The secondary

suspension bogie is connected to each set of wheelset by one set of K_s and C_s. In addition, the

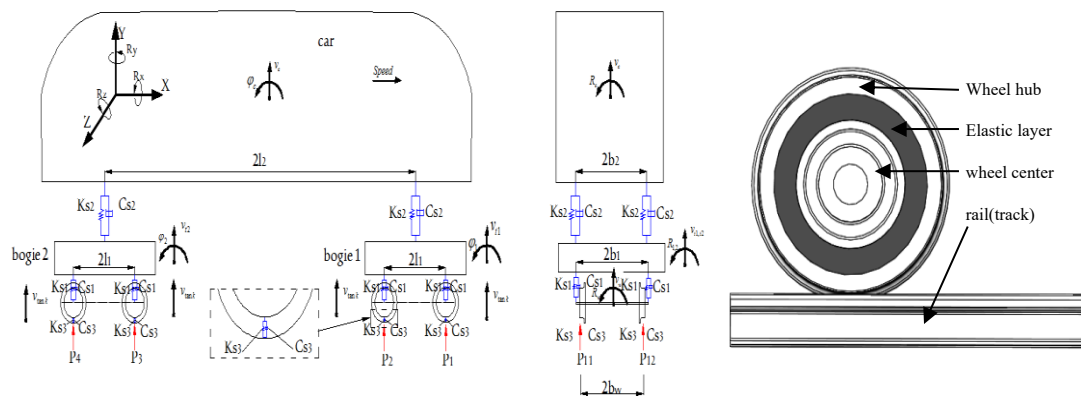mass, moment of inertia, and dimension parameters of the system are defined.

Figure1. Three-dimensional model of train system. The black arrow indicates the degree of freedoms for the key components. Subscript c, t, $\tan k$ represents carriage, bogie, wheel orderly. Blue components represent spring and damping.

According to the concept of dynamic balance and D'Alembert's principle[9], the dynamic

equations of motion of different components of the railway system are derived. The dynamic

equations are in the form of second-order differential equations in time and displacement domain.

Van, Dinha et al. studied the form of the dynamic equation for the coupling of a three-dimensional

train system and bridge track. Considering the addition of elastic wheels and the change of degrees

of freedom of the system, the dynamic equations are rewritten in this study. The specific equations

of each component of the whole vehicle system are as follows: v represents displacement, $\dot{v}$

represents speed, $\ddot{v}$ represents acceleration. c, t, w represent carriage, bogie and wheel respectively.

We now define key dynamic balances:

The dynamic balance of vertical motion in y-axis of carriage is,

$$M_c\ddot{v}_c + \left(4\dot{v}_c - 2\dot{v}_{t1} - 2\dot{v}_{t2}\right)C_{S2} + \left(4v_c - 2v_{t1} - 2v_{t2}\right)K_{S2} = 0 \tag{1}$$

Dynamic balance of rolling motion in z-axis of carriage is,

$$J_{cz}\dot{\varphi}_c + \left(4\dot{\varphi}_c l_2 + 2\dot{v}_{t1} - 2\dot{v}_{t2}\right)C_{S2}l_2 + \left(4\varphi_c l_2 + 2v_{t1} - 2v_{t2}\right)K_{S2}l_2 = 0 \tag{2}$$

Dynamic balance of rolling motion in x-axis of carriage is,

$$J_{cx}\ddot{R}_c + \left(4\dot{R}_c b_2 - 2\dot{R}_{t1}b_2 - 2\dot{R}_{t2}b_2\right)C_{S2}b_2 + \left(4R_c b_2 - 2R_{t1}b_2 - 2R_{t2}b_2\right)K_{S2}b_2 = 0 \tag{3}$$

where φ represents the angle of the pitching motion; R represents the angle of the rolling motion.

Dynamic balance of vertical movement in y-axis of bogie i is,

$$\begin{aligned}
&M_t\ddot{v}_{ti} + (2C_{S2} + 4C_{S1})\dot{v}_{ti} - 2C_{S2}\dot{v}_c - 2C_{S1}\dot{v}_{wj} + (-1)^i 2l_2 C_{S2}\dot{\varphi}_c \\
&+ (2K_{S2} + 4K_{S1})v_{ti} - 2K_{S2}v_c - 2K_{S1}v_{wj} + (-1)^i 2l_2 C_{S2}\varphi_c = 0
\end{aligned} \quad i = 1,2 \; j = 1,2,3,4 \tag{4}$$

Dynamic balance of rolling motion in z-axis of bogie i is,

$$J_{tz}\ddot{\varphi}_{ti} + 4l_1^2 C_{S1}\dot{\varphi}_{ti} - 2C_{S1}l_1\dot{v}_{wj} + 4l_1^2 K_{S1}\varphi_{ti} - 2l_1 K_{S1}v_{wj} = 0 \quad i = 1,2 \; j = 1,2,3,4 \tag{5}$$

Dynamic balance of rolling motion in x-axis of bogie i is,

$$J_{tx}\ddot{R}_i + \left(2b_1^2 C_{S2} + 4b_1^2 C_{S1}\right)\dot{R}_i - 2b_1^2 C_{S2}\dot{R}_c - 2b_1^2 C_{S1}\dot{R}_{\omega j}$$
$$+\left(2b_1^2 K_{S2} + 4b_1^2 K_{S1}\right)R_i - 2b_1^2 C_{S2}R_c - 2b_1^2 K_{S1}R_{\omega j} = 0 \qquad i=1,2 \quad j=1,2,3,4 \qquad (6)$$

where b_1 represents the lateral distance of left and right wheels.

Dynamic balance of vertical movement in y-axis of wheelset j is,

$$M_w\ddot{v}_{wj} + \left(2C_{s1}+2C_{s3}\right)\dot{v}_{wj} - 2C_{s1}\dot{v}_{ti} - C_{s3}\dot{v}_{\tan k_{q1}} - C_{s3}\dot{v}_{\tan k_{q2}}$$
$$+\left(2K_{s1}+2K_{s3}\right)v_{wj} - 2K_{s1}v_{ti} - K_{s3}v_{\tan k_{q1}} - K_{s3}v_{\tan k_{q2}} = 0 \qquad j=1,2,3,4 \qquad (7)$$

where j represents the location of the wheelsets, and q1, q2 represent the left and right wheels.

Dynamic balance of rolling motion x-axis of wheelset j is,

$$J_{wx}\ddot{R}_{wj} + (2b_w^2 C_{s1} + 2b_w^2 C_{s3})\dot{R}_{wj} - 2b_w^2 C_{s1}\dot{R}_{ti} - b_w^2 C_{s3}\dot{v}_{\tan k_{q1}} + b_w^2 C_{s3}\dot{v}_{\tan k_{q2}}$$
$$+(2b_w^2 K_{s1} + 2b_w^2 K_{s3})R_{wj} - 2b_w^2 K_{s1}R_{ti} - b_w^2 K_{s3}v_{\tan k_{q1}} + b_w^2 K_{s3}v_{\tan k_{q2}} = 0 \qquad i=1,2 \quad j=1,2,3,4 \qquad (8)$$

Dynamic balance of vertical movement in y-axis of wheel hub k_{q1} is,

$$M_{\tan}\ddot{v}_{\tan k_{q1}} + C_{s3}\dot{v}_{\tan k_{q1}} - C_{s3}\dot{v}_{wj} + b_\omega C_{s3}\dot{R}_{wj} + K_{s3}v_{\tan k_{q1}} - K_{s3}v_{wj} + b_\omega K_{s3}R_{wj} = P_{\tan k_{q1}} \qquad k=1,2,3,4$$

$$(9)$$

Dynamic balance of vertical movement in y-axis of wheel hub k_{q2} is,

$$M_{\tan}\ddot{v}_{\tan k_{q2}} + C_{s3}\dot{v}_{k_{q2}} - C_{s3}\dot{v}_{w1} - b_\omega C_{s3}\dot{R}_{wj} + K_{s3}v_{\tan k_{q2}} - K_{s3}v_{wj} - b_\omega K_{s3}R_{wj} = P_{\tan k_{q2}} \qquad j=1,2,3,4$$

$$(10)$$

where k represents the location of wheel hub.

According to the theory of dynamics, the motion equation of the whole vehicle system can be written in a general form,

$$[\mathbf{M}]\{\ddot{V}\}+[C]\{\dot{V}\}+[K]\{V\}=\{\mathbf{P}\} \tag{11}$$

where M, C and K are the total mass, damping and stiffness matrices of the vehicle.

The displacement vector of the whole vehicle system is as follows,

$$\{\mathbf{V}\}=\left\langle V_c \quad V_{t1} \quad V_{t2} \quad V_{\omega1} \quad V_{\omega2} \quad V_{\omega3} \quad V_{\omega4} \quad V_{tan} \right\rangle^T$$

$$\{\mathbf{V_c}\}=\left\langle v_c \quad \varphi_c \quad R_c \right\rangle^T, \{\mathbf{V}_{ti}\}=\left\langle v_{ti} \quad \varphi_{ti} \quad R_{ti} \right\rangle^T \tag{12}$$

$$\{\mathbf{V}_{\omega j}\}=\left\langle v_{\omega j} \quad \varphi_{\omega j} \quad R_{\omega j} \right\rangle^T, \{\mathbf{V}_{tan}\}=\left\langle v_{tan\,k_{q1}} \quad v_{tan\,k_{q2}} \right\rangle^T$$

The mass matrix of the vehicle is as follows,

$$[\mathbf{M}]=diag\left[M_c \quad M_{t1} \quad M_{t2} \quad M_{\omega1} \quad M_{\omega2} \quad M_{\omega3} \quad M_{\omega4} \quad M_{tan}\right]$$

$$[\mathbf{M_c}]=diag\left[M_c \quad J_{cz} \quad J_{cx}\right], [\mathbf{M}_{ti}]=diag\left[M_{ti} \quad J_{tzi} \quad J_{txi}\right] \tag{13}$$

$$\left[\mathbf{M}_{\omega j}\right]=diag\left[M_{\omega j} \quad J_{\omega xj}\right], [\mathbf{M}_{tan\,k}]=diag\left[M_{tan\,k}\right]$$

The stiffness matrix of the vehicle is as follows,

$$[\boldsymbol{K}]=\begin{bmatrix} K_c & K_{ct1} & K_{ct2} & 0 & 0 & 0 & 0 & 0 \\ K_{ct1} & K_{t1} & 0 & K_{t1w1} & K_{t1w1} & 0 & 0 & 0 \\ & K_{t2} & 0 & 0 & K_{t2w3} & K_{t2w4} & 0 \\ & & K_{w1} & 0 & 0 & 0 & K_{w1\,tan\,k} \\ & & & K_{w2} & 0 & 0 & K_{w2\,tan\,k} \\ & & & & K_{w3} & 0 & K_{w3\,tan\,k} \\ & & & & & K_{w4} & K_{w4\,tan\,k} \\ sym & & & & & & K_{tan\,k} \end{bmatrix} \tag{14}$$

$\boldsymbol{K}_c$, $\boldsymbol{K}_{ti}$, $\boldsymbol{K}_{\omega j}$ and $\boldsymbol{K}_{tan\,k}$ are the stiffness matrix of the body, the i th bogie, the j th wheelset and

the k th elastic wheel hub respectively. $\boldsymbol{K}_{cti}$ is the stiffness matrix connecting the body and the first

bogie. $\boldsymbol{K}_{ti\omega j}$ is the stiffness matrix connecting the i th bogie and the j th wheelset. $\boldsymbol{K}_{\omega j\,tan\,k}$ is the

stiffness matrix connecting the j th wheel pair with the k th elastic wheel hub.

The damping matrix of the whole vehicle C is obtained by a method similar to the stiffness matrix K.

The external dynamic load vector applied into the whole vehicle is written as,

$$\{\mathbf{P}\} = \langle P_c \quad P_{t1} \quad P_{t2} \quad P_{\omega 1} \quad P_{\omega 2} \quad P_{\omega 3} \quad P_{\omega 4} \quad P_{\tan k} \rangle^T \tag{15}$$

where P_c, P_{ti}, $P_{\omega j}$ and $P_{\tan k}$ are the load vectors applied to the train body, the i th bogie and the j th wheelset, the wheel-rail force. In addition, the gravity of the wheel $G_{\tan k}$ is considered as a static load of the railway system. Since the current study does not consider the effect of external forces, therefore,

$$\{P_c\} = \{0\}, \{P_{ti}\} = \{0\}, \{P_{\omega j}\} = \{0\}, \{P_{\tan k}\} = \{P_{\tan k}\}$$

$$G_{\tan k} = (0.125M_c + 0.25M_t + 0.5M_w + M_{\tan})g \tag{16}$$

2.2 Wheel-rail force

The function of the elastic layer between the wheel center and the hub is elastic deformation and damping of wheel. The existence of damping absorbs a part of the impact energy during the wheel-rail contact process. The elastic layer is equivalent to the combination of linear compressive spring and viscous damper. During the process of wheel-rail contact, the wheel center generates pressure in the negative direction of the track surface due to the gravity. The lower part of the elastic layer bears the load, while the upper part only bears the pre-tightening force in the assembly of parts.

Only the bearing capacity of the lower part of the elastic layer is considered in the modeling process, and the specific structure is shown in Figure 3.

A variety of mathematical and numerical models are available to define wheel-rail contact, including longitudinal creep, friction behavior, braking/traction and hysteresis damping characteristics in contact problems, which seen in the literature[10-16]. In this paper, a Hertzian elastic contact model is used to simulate wheel-rail contact. In particular, when studying the wheel-rail contact problem，a finite element model of wheel-rail contact region is often established, and the contact circle is divided into small units, where the wavelength is less than the cell length to ensure that the result is valid. This paper studies the vibration of the railway system through the dynamic equation of the whole vehicle system, where the track is simplified into continuous irregularity excitation points. The research is based on the following assumptions.

a. No contact damping/hysteretic material damping during wheel-rail contact.

b. The result is an isothermal solution.

c. The ripples are regular.

d. There is no longitudinal creep.

e. There is braking/traction behavior.

f. The wheel hub and railtrack are the same material.

g. There is frictionless contact between wheels and rails.

A roughness on top of the waviness could have been used to create a dry friction model, which was used to assume Gaussian distribution of asperity peaks and non-Gaussian roughness, typical of steel engineering surfaces, which seen in the literature[17,18].

The wheel-rail normal contact stiffness is expressed as KH, and the contact force between the wheel hub and the rail is $P_{\tan k}$, which is derived from the Hertz theory of normal elastic contact.

$$KH = \frac{2}{3} \frac{E}{1-\mu} (r_\omega r_r)^{1/4} \tag{17a}$$

where E is the Young's modulus, and μ is the Poisson's ratio.

$$P_{\tan k} = \begin{cases} KH\left(v_{\tan k}^{w-r}\right)^{3/2}, & v^{w-r} < 0 \\ 0, & v^{w-r} \geq 0 \end{cases} \tag{17b}$$

where $v_{\tan k}^{w-r}(t)$ is the relative displacement of the k th wheel hub to the track, which can be expressed as,

$$v_{\tan k}^{w-r}(t) = v_k^w(t) - IR_y(xk) \tag{18}$$

where $v_k^w(t)$ is the displacement of the k th elastic hub, $IR_y(xk)$ represents the rail irregularity value at the contact point x between k th wheel hub and the track.

The wheel-rail contact force $P_{\tan k}$ is nonlinear in Figure 2. In this paper, the maximum fluctuation range of the relative displacement of wheel hub to the track $v_{\tan k}^{w-r}(t)$ is less than 0.05mm, which is relatively small; therefore the wheel-rail contact force $P_{\tan k}$ is approximated to be linear.
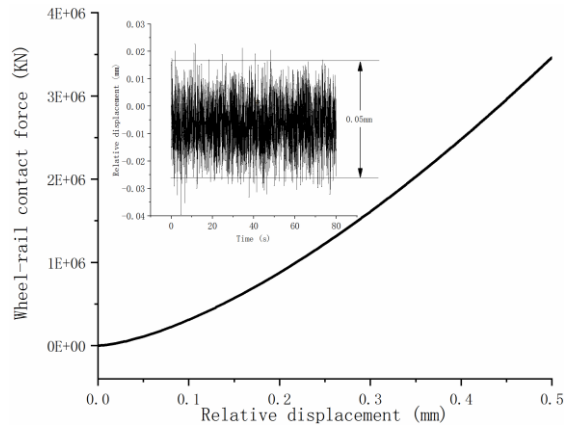
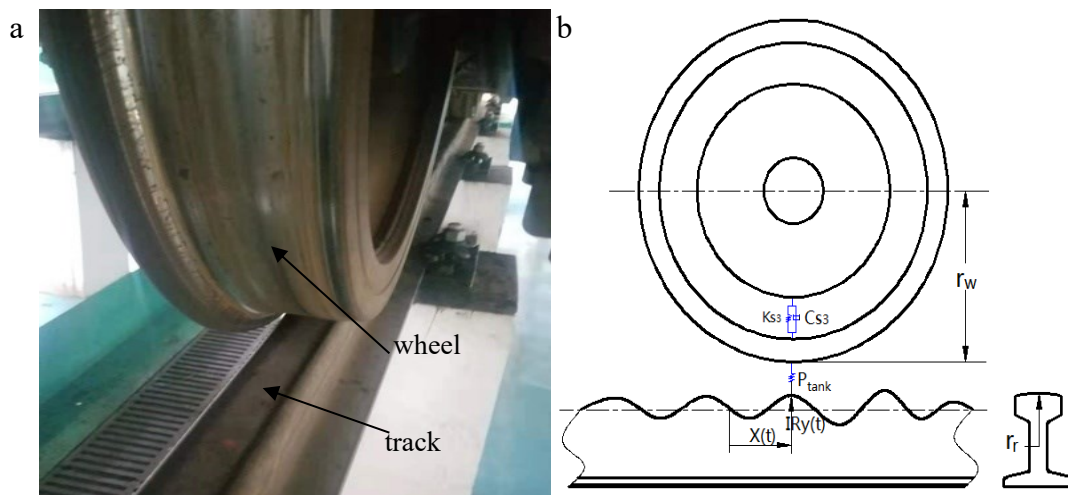**Figure 2.** Relationship between wheel-rail contact force and the relative displacement of the hub to the rail.

Figure 3. Wheel-rail relationship of elastic wheel,(a) real object, (b) schematic diagram.

where K_{s3} , C_{s3} represent stiffness coefficient and damping coefficient of elastic layer, $X(t)$ represents the distance that the wheel traveled at any time in a time step $\Box t$, and $P_{\tan k}$ represents the wheel-rail force. In this study, the Newmark-β method has been adopted to calculate by time

domain integration, which is unconditionally stable, with a time step $\Box t$ of 0.001s and the sampling step of track irregularity is 0.001s. The time step of this calculation is consistent with the sampling step of track irregularity, which ensures accuracy of the calculated result.

2.3 Analysis parameters and track irregularity

The development direction of urban rail vehicles is high speed, light-weight and low-noise. In order to adapt to the development in the future, this research considers a Chinese HSC high-speed railway vehicle as the prototype. The parameters of the vehicle body parameters are obtained from the literature[2], and elastic wheel components are added, and the weight of railway system and wheel parameters are adjusted. The vehicle body parameters required in the simulation process are shown in the table 1.

Table 1. Parameters of the vehicle body parameters employed in the numerical analysis.

Notation	Parameter	Value	Unit
g	Gravitational acceleration	9.8	N/kg
M_c	Mass of car	52000	kg
J_c	Car moment of inertia（z,x）	$2.31\times10^6, 1.31\times10^6$	$kg\Box m^2$
M_t	Mass of bogie	1600	kg
J_{tz}, J_{tx}	Bogie moment of inertia（z,x）	3120, 2120	$kg\Box m^2$
M_w	Mass of wheelset	1400	kg
J_{wx}	Wheelset moment of inertia	1220	$kg\Box m^2$
$M_{\tan}$	Mass of elastic wheel	300	$kg\Box m^2$
K_{s1}	Primary suspension stiffness	1.87×10^3	N/m
K_{s2}	Secondary suspension stiffness	1.72×10^3	N/m
C_{s1}	Primary suspension damping	500	$N\Box s/m$
C_{s2}	Secondary suspension damping	500	$N\Box s/m$
C_{s3}	tertiary suspension damping	270	$N\Box s/m$
l_1, l_2	Size of length	1.25,9	m
b_1, b_2, b_w	Size of width	1.25,2,1.5	m

r_r	head radius of rail cross section	0.3	m
r_w	Wheel rolling radius	0.45	m
E	Young's moduluselastic ratio	2.06×10^5	N/mm^2
μ	Poisson's ratio	0.3	

The effect of stiffness coefficient K_{s3} of elastic layer on vertical acceleration of wheel is studied under the same track irregularity. The relationship between K_{s3} and vertical acceleration of wheel can be examined where the initial stiffness coefficient of the elastic layer is set as 1.42×10^3 N/m, with a gradual increase of 0.2×10^3 N/m, leading to 12 groups of data for calculation and comparison and the change of K_{s3} is shown in the table 2. The initial stiffness coefficient is set as 1.42×10^3 N/m, which is defined by multiple experiments and if the value is too small, the solution of system will be divergent.

Table 2. Parameters of the stiffness coefficients K_{s3} of elastic wheel.

Number	Stiffness coefficient（N/m）	Number	stiffness coefficient（N/m）
1	1.42×10^3	7	2.62×10^3
2	1.62×10^3	8	2.82×10^3
3	1.82×10^3	9	3.02×10^3
4	2.02×10^3	10	3.22×10^3
5	2.22×10^3	11	3.42×10^3
6	2.42×10^3	12	3.62×10^3

In many studies, track irregularity is considered an important source of vehicle body dynamic excitation[19-24]. In this study, the United States six track irregular spectrum is selected, which includes three frequency bands from 500 to 1100Hz, 700 to 1300Hz, 900 to 1500Hz. The irregularity

in frequency domain is transformed into three groups of random response variables in time domain

as irregularity excitation through inverse the Laplace transform, the values of irregularity excitation

near 0.2mm,0.1mm,0.08mm orderly, as shown in the Figure 4. The power density function of track

irregularity excitation as follows,

$$S_v(\omega) = \frac{kA_v\omega_c^2}{(\omega^2 + \omega_c^2)\omega^2} \tag{19}$$

where $S_v(\omega)$ is the power density function ($cm/rad/m$), ω is the spatial frequency (rad/m), ω_c

is the truncation frequency(rad/m), and A_v is the roughness coefficient ($cm\square rad/m$).
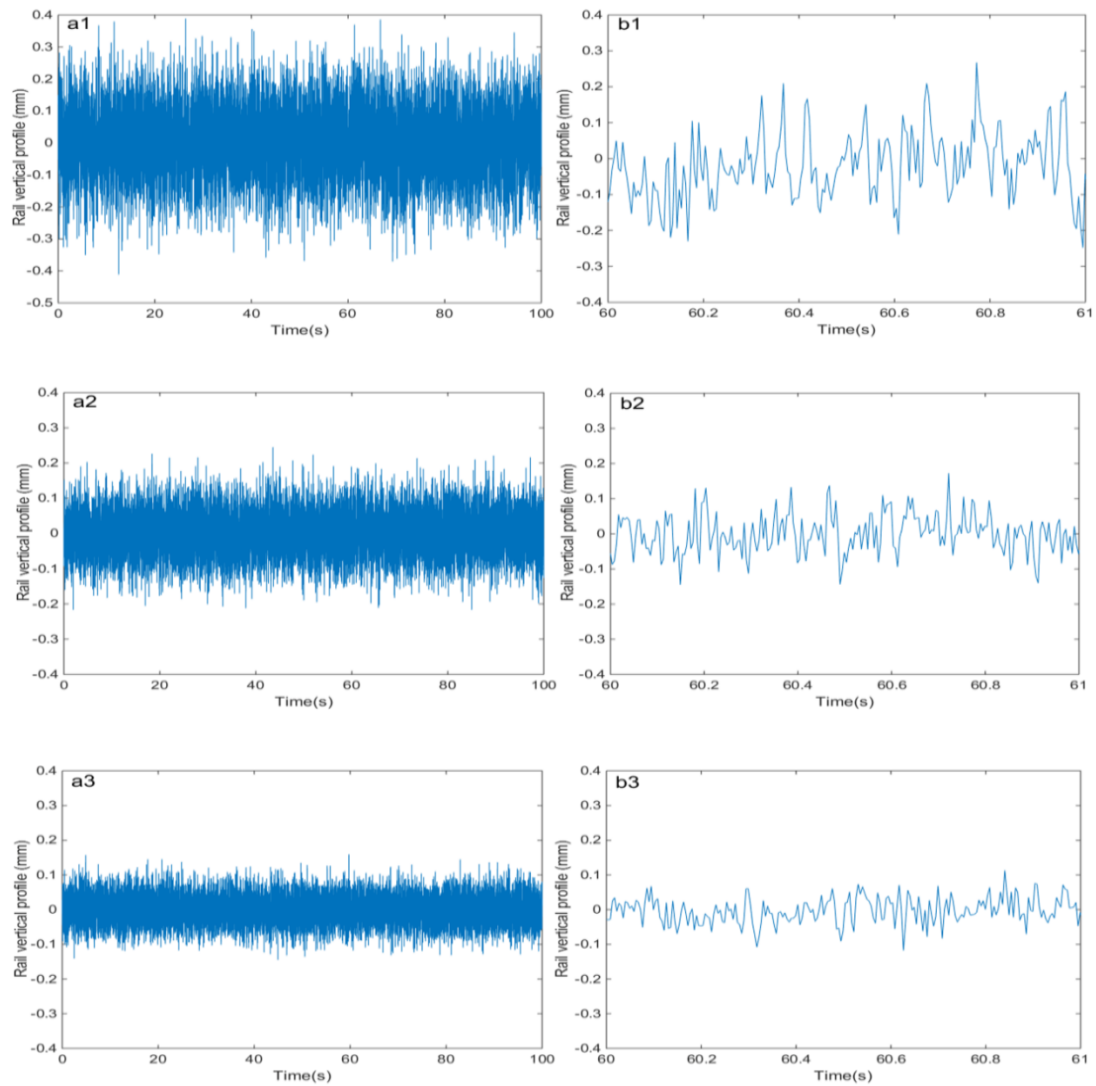
Figure 4. Three types of track irregularity conditions, (a) entire simulation, (b) magnification at a limited time zone. (1,2,3 means the power density spectrum frequency of 500-1100,700-1300,900-1500. The degree of track irregularity near 0.2mm,0.1mm,0.08mm orderly.)

In order to verify the accuracy of dynamic simulation model, vehicle and track dynamics

parameters are defined from the literature [2], the variation of wheel-rail force is calculated under

three kinds of 'V-shaped' defect conditions and are calculated based on the model and program in this paper. As shown in Figure 5, the fluctuations increase in turn with the increase of the V-shaped defect value. This is consistent with the variation trend of wheel-rail forces in the literature [2], indicating confidence in model.
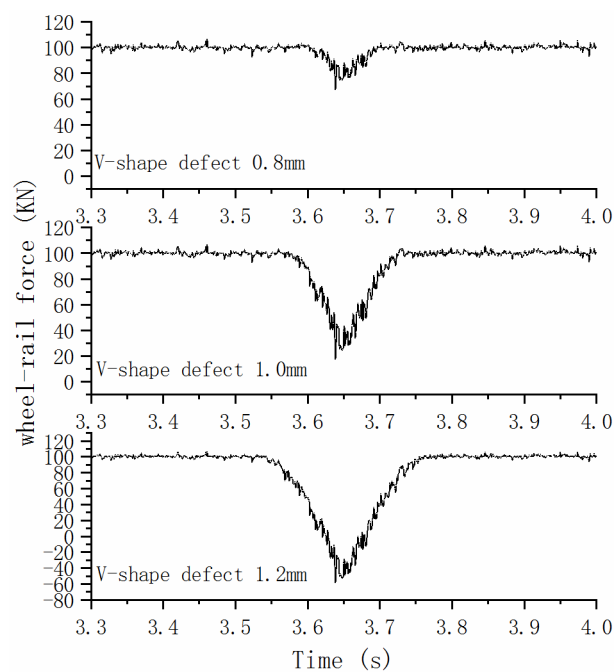

Figure 5. Wheel-rail contact force under three kinds of V-shaped defect conditions.

3 Calculation and results

3.1 Calculation method

The equations are solved using the numerical time integration method of Newmark-β in present research. Using displacement as the initial variable, the velocity and acceleration are calculated by matrix iteration. Due to the significant savings in computing time, this method is popular for

numerical integration of structural dynamics equations, especially in nonlinear systems[25,26]. In

the Newmark-β numerical integral method, when velocities of the system is v_t、$\dot{v}_t$、$\ddot{v}_t$, velocities

of the next time $v_{t+\Delta t}$, $\dot{v}_{t+\Delta t}$, $\ddot{v}_{t+\Delta t}$ can be acquired by the following formula:

$$(K + c_0 M + c_1 C)v_{t+\Delta t} = P_{t+\Delta t} + M(c_0 v_t + c_2 \dot{v}_t + c_3 \ddot{v}_t) + C(c_1 v_t + c_4 \dot{v}_t + c_5 \ddot{v}_t)$$

$$\dot{v}_{t+\Delta t} = \dot{v}_t + c_6 \ddot{v}_t + c_7 \ddot{v}_{t+\Delta t}, \ddot{v}_{t+\Delta t} = c_0(\dot{v}_{t+\Delta t} - v_t) - c_2 \dot{v}_t - c_3 \ddot{v}_t \tag{20}$$

where parameters are defined as

$$c_0 = \frac{1}{\alpha \Delta t^2}, c_1 = \frac{\delta}{\alpha \Delta t}, c_2 = \frac{1}{\alpha \Delta t}, c_3 = \frac{1}{2\alpha} - 1, c_4 = \frac{\delta}{\alpha} - 1$$

$$c_5 = \frac{\Delta t}{2}(\frac{\delta}{\alpha} - 2), c_6 = \Delta t(1 - \delta), c_7 = \delta \Delta t \tag{21}$$

where Δt is the time step, α and δ are the numerical integration parameters, which are

generally taken as 0.25 and 0.5.

In order to avoid derailment phenomenon in the vertical direction, a constraint is defined as the

following formula:

$$\left| v_{t+\Delta t}^{i+1} - v_{t+\Delta t}^{i} \right| \leq \left| IR_y^{i+1}(xk) - IR_y^{i}(xk) \right| \tag{22}$$

where the left is the absolute value of the wheel displacement between adjacent time nodes, the right

is the absolute value of the displacement between adjacent irregularity values. If the constraint in

not satisfied, the wheel-rail contact force $P_{\tan k}$ is recalculated by formula 17, and the new wheel

displacement is verified.

On this basis, the program code based on MATLAB is compiled to solve the equations. The real-time motion results of the railway system are stored in the form of matrix and the vertical response of the wheel at each time step is calculated. The program structure is shown in Figure 6.
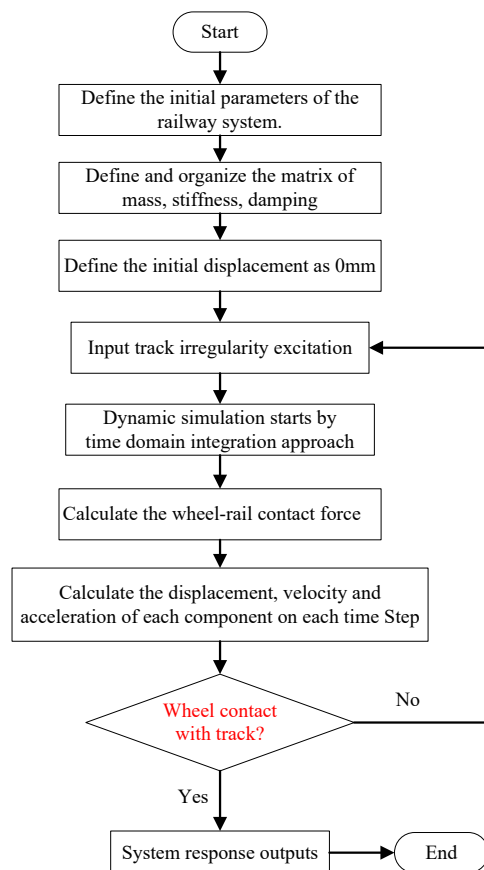

Figure 6. Process structure of dynamic simulation.

3.2 Calculation results

According to the given irregularity excitation and the increasing stiffness coefficient of the elastic layer, the movement of whole vehicle system is simulated. In order to study the influence of track

irregularity and stiffness coefficients of elastic layer on wheel vibration, we obtain the motion characteristics of each component of the railway system at adjacent time nodes, which can be used to find the specific time node and orbit position corresponding to the maximum value of vibration; as a result the time history curve of wheel vertical acceleration is obtained. For different levels of track irregularity, the change of vertical acceleration of the wheel is shown in the Figure 7 to 9. For different stiffness coefficients of elastic layer, the change of vertical acceleration of wheels is shown in the Figure 10 to 12. In addition, a larger view of a finite time zone is shown to better compare the calculated results, and the change of vertical maximum acceleration, minimum acceleration and average acceleration are obtained.
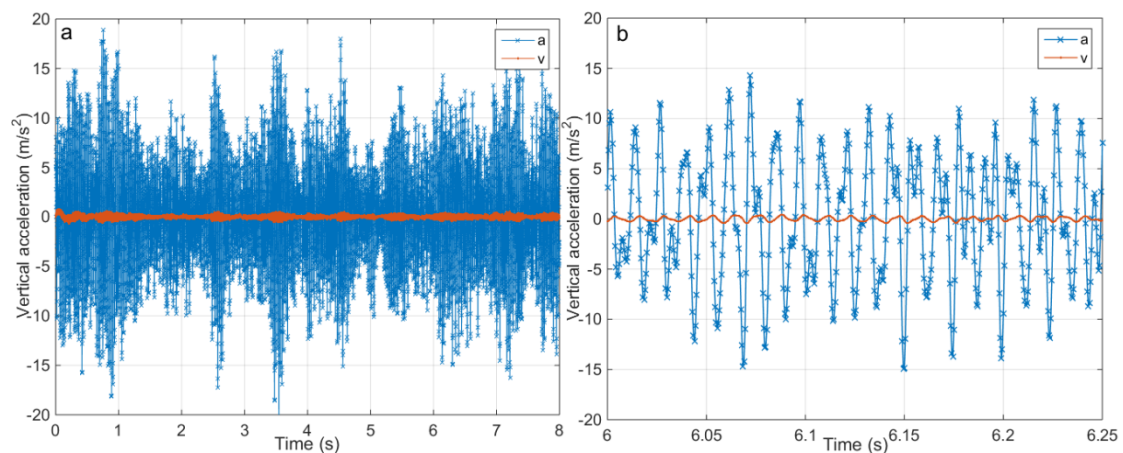

Figure7. Wheel vertical acceleration when track irregularity spectrum is 500-1100(condition 1), (a) entire simulation, (b) magnification at a limited time zone. The red curve shows the change of vertical speed v, the blue curve shows the change of vertical acceleration a.
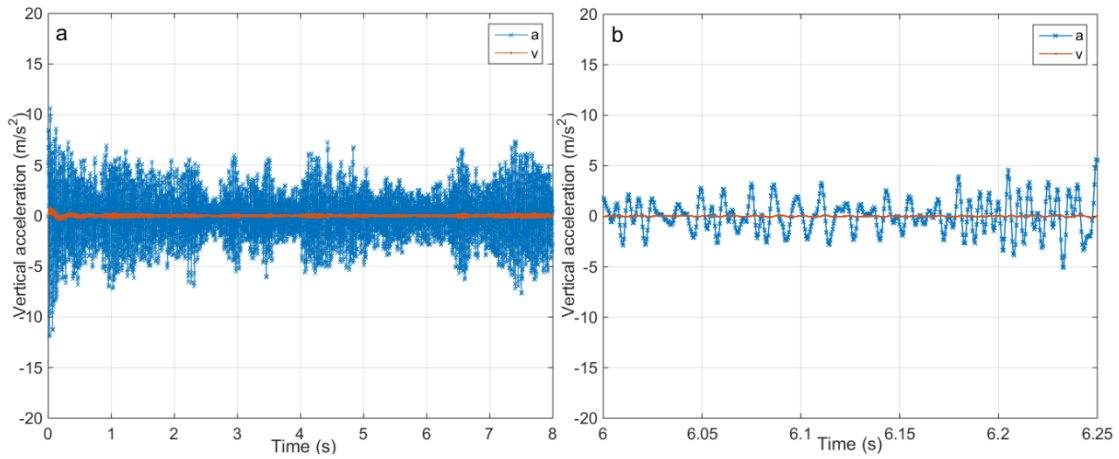
Figure8. Wheel vertical acceleration when track irregularity spectrum is 700-1300(condition 2), (a) entire simulation, (b) magnification at a limited time zone. The red curve shows the change of vertical speed v, the blue curve shows the change of vertical acceleration *a*.
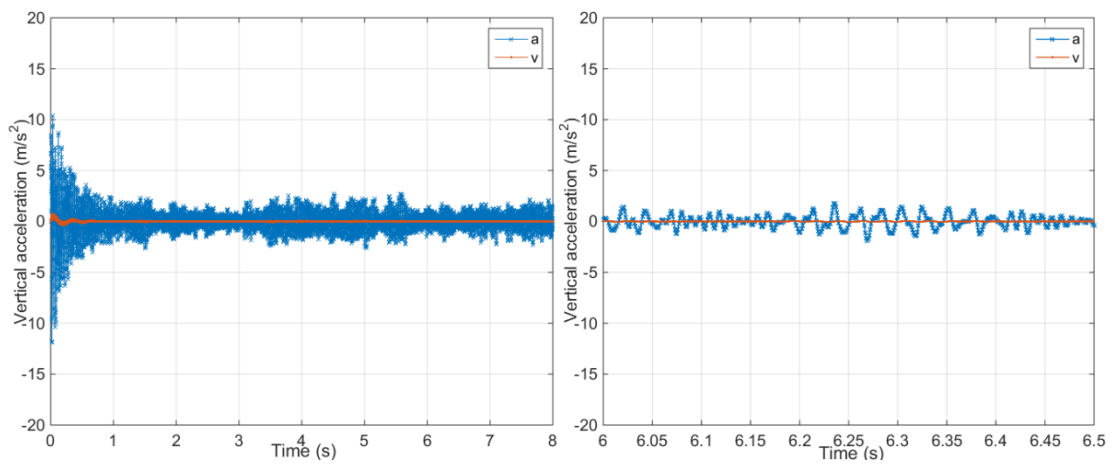

Figure9. Wheel vertical acceleration when track irregularity spectrum is 900-1500(condition 3), (a) entire simulation, (b) magnification at a limited time zone. The red curve shows the change of vertical speed v, the blue curve shows the change of vertical acceleration *a*.
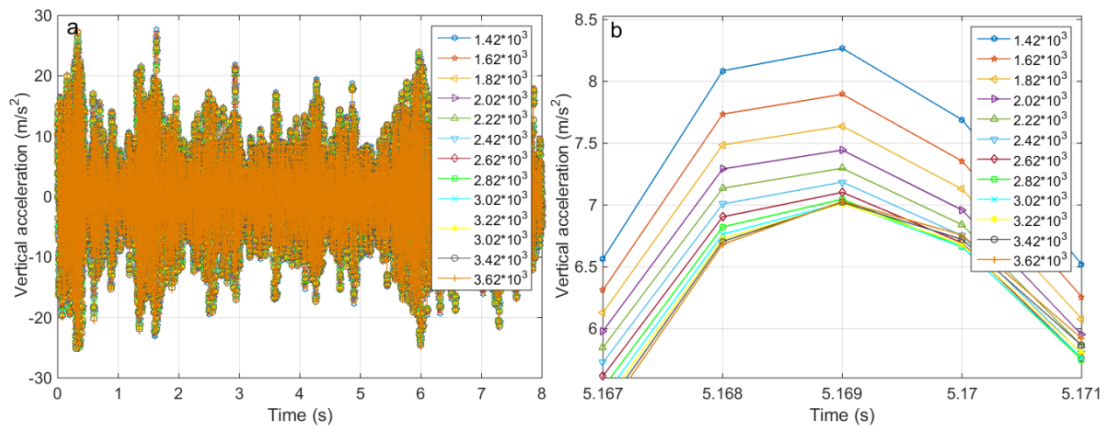
Figure 10. Wheel vertical acceleration with the change of stiffness coefficient when track irregularity spectrum is 500-1100(condition 1), (a) entire simulation, (b) magnification at a limited time zone. The color distinguishes the multiple stiffness coefficients of wheels in Table 2.

Figure 11. Wheel vertical acceleration with the change of stiffness coefficient when track irregularity spectrum is 700-1300(condition 2), (a) entire simulation, (b) magnification at a limited time zone. The color distinguishes the multiple stiffness coefficients of wheels in Table 2.
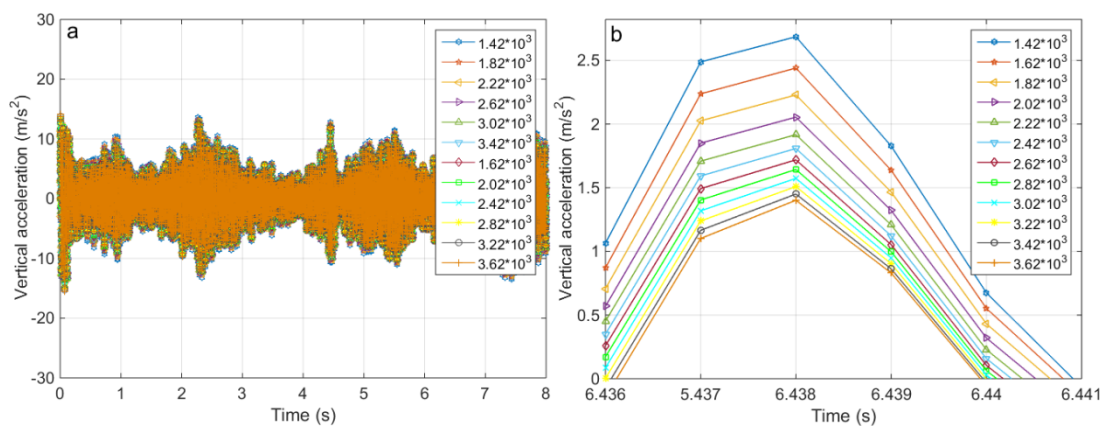
Figure 12. Wheel vertical acceleration with the change of stiffness coefficient when track irregularity spectrum is 900-1500(condition 3),(a) entire simulation, (b) magnification at a limited time zone. The color distinguishes the multiple stiffness coefficients of wheels in Table 2.
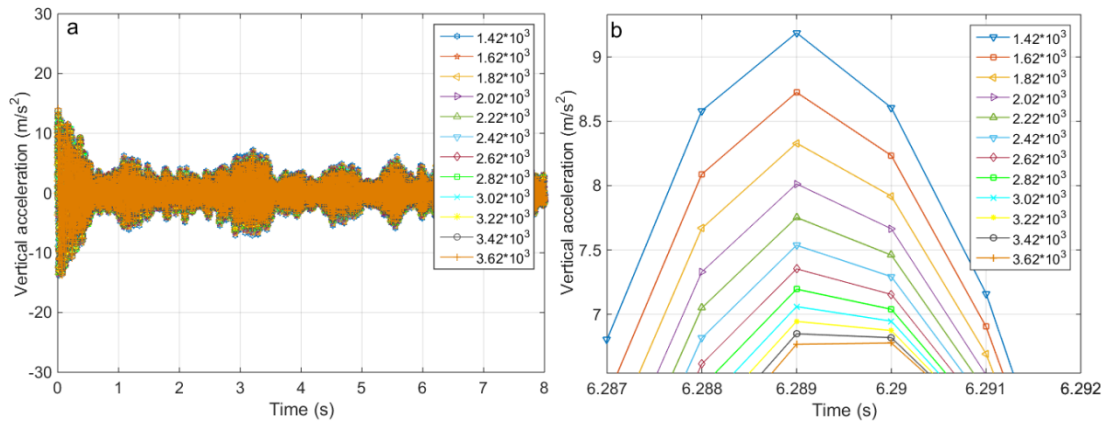
3.3 Discussion

Figures 7 to 9 show the changes of the vertical acceleration and vertical velocity of the wheel. It can be seen as the irregularity of track gradually decreases from 0.2mm to 0.1mm, and then to 0.08mm, the fluctuation of vertical acceleration changes from ($-15m/s^2 \sim +15m/s^2$) to($-8m/s^2 \sim +8m/s^2$), and then to ($-4m/s^2 \sim +4m/s^2$) respectively, which indicates that the influence of track irregularity is significant on the vertical acceleration of wheels. In addition, the vertical acceleration of the wheels reduces with the reduction of track irregularity. However, the change of the vertical velocity of the wheel is not significant.

In Figures 10 to 12, the influence of stiffness coefficient of elastic layer is examined on the vertical acceleration of the wheel. With a decrease of track irregularity, the vertical distance between the

vertical acceleration curves $1.42 \times 10^3 \text{m/s}^2$ and $3.62 \times 10^3 \text{m/s}^2$ decreases successively. The influence of the stiffness coefficient of the elastic wheel on the vertical acceleration weakens with reduction of track irregularity. In addition, the vertical distance between the adjacent curves decreases gradually, which indicates that the relationship between the stiffness coefficient of the elastic layer and the vertical acceleration of the wheel is non-linear.

By comparing the results of the Figure 13, it can be seen that the fluctuation coefficient of the vertical acceleration exhibits a spring-back trend (i.e. it initially decreases gradually, and then increases gradually after reaching the minimum value with an increase of the stiffness coefficient of the elastic layer). Furthermore, the lower the track irregularity, the lower the degree of spring-back. It can be observed that there is an obvious spring-back when the track irregularity is 0.2mm, with a significant reduction of spring-back when the track irregularity is 0.1mm, and a very small degree of spring-back when the track irregularity is only 0.08mm. The reason for this phenomenon is that the elastic layer does not have sufficient supporting capacity when the stiffness coefficient is small. In addition, the hub is no longer in close contact with elastic layer, which causes an increase in the vertical acceleration fluctuation. When the stiffness coefficient is too large, the deformability of the elastic layer is weakened and the impact produced by the track irregularity cannot be absorbed, which intensifies the vertical acceleration. In addition, the fluctuation coefficient of the vertical acceleration reaches a minimum value when the stiffness coefficient of the elastic layer nears

2.1×10^3 N/m, 3.0×10^3 N/m, 3.3×10^3 N/m in sequence for different track irregularity. The comprehensive analysis shows that the stiffness coefficient increases gradually corresponding to the minimum of fluctuation coefficient with the reduction of track irregularity. Thus, in order to minimize the fluctuation coefficient, the degree of track irregularity should be reduced and the stiffness coefficient should be increased correspondingly.

Figure 14 shows the range of wheel vertical accelerations. It can be seen that the range of vertical acceleration falls with a reduction of track irregularity. Furthermore, the range of vertical acceleration exhibits a V-shaped trend and reaches a minimum when the stiffness coefficient of the elastic layer is approximately 2.4×10^3 N/m. For different system parameters, the stiffness coefficient must be different when the range of wheel vertical acceleration reaches the minimum value, but the overall trends are similar. Therefore, a reasonable range of stiffness coefficients can be obtained by combining the specific system parameters.
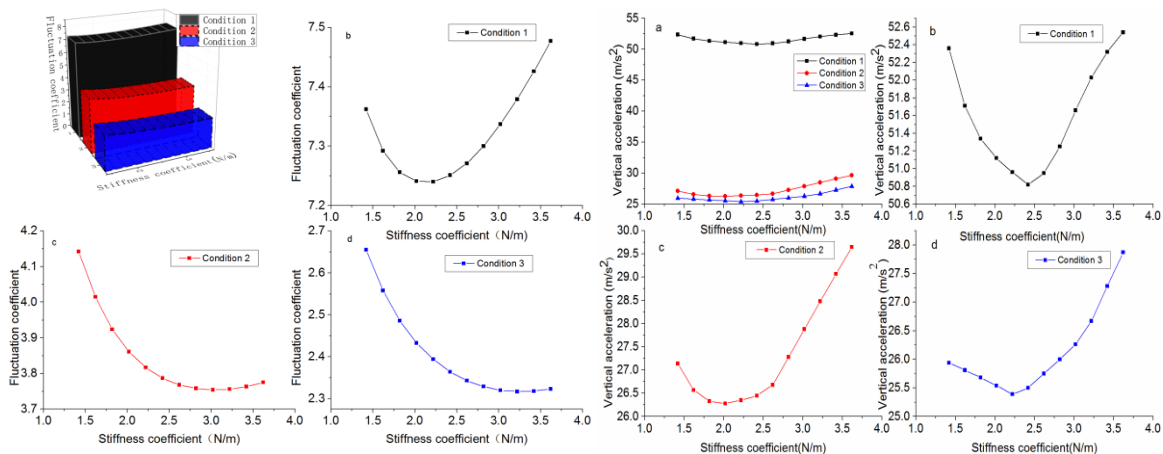
Figure 13. Fluctuation coefficient of wheel vertical acceleration,(a) compare three conditions,(b,c,d) condition 1,2,3.

Figure 14. Range of wheel vertical acceleration, (a) compare three conditions, (b,c,d) local enlarged view for condition 1, 2,3.

According to the maximum, minimum and the average value of vertical acceleration in Figure 15, it can be seen that the maximum vertical acceleration increases and minimum vertical acceleration value decreases with an increase of track irregularity in the sequence. According to comparing the results of condition 2 and condition 3, the smaller the stiffness coefficient of the elastic layer, the more easily the maximum value of vertical acceleration of the wheel is affected by the track irregularity. The larger the stiffness coefficient, the more easily the minimum value of vertical acceleration of the wheel is affected by the track irregularity. The main reason for this phenomenon is that the wheel displaces more on the positive direction of the track contact surface when the stiffness coefficient of elastic layer is relatively small, which results in an increase in fluctuation of the maximum value. As the stiffness coefficient of elastic layer increases, the rigidity of the wheel increases and more load will be consumed by the compression deformation of the track when wheel-rail contact, the wheel displaces more on the negative direction of the track contact surface, leading to greater fluctuation of the minimum vertical acceleration.

From the local enlarged view of average value in the Figure 16, it can be seen that the average value of the vertical acceleration exhibits an S-shaped trend with an increase of the stiffness coefficient. However, the S-shape gradually transforms to a linear relationship with a decrease of track irregularity.
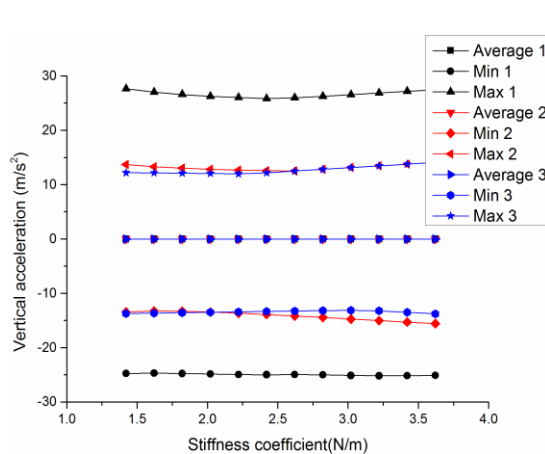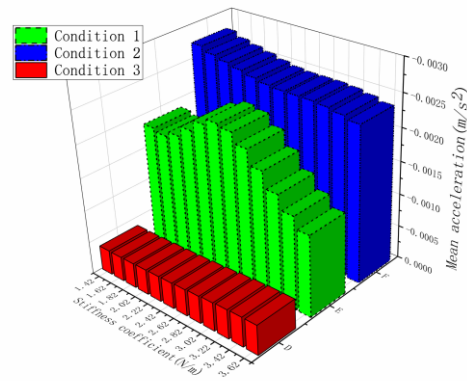
Figure 15. Wheel vertical acceleration.

Figure 16. The local enlarged view of average value about wheel vertical acceleration.

4 Conclusion

A detailed dynamic model of railway vehicle with elastic wheel damping structure is established, and the effect of stiffness coefficient of elastic wheel and track irregularity on wheel-rail coupling vibration has been studied using the new dynamic model. Taking an urban railway system as the research object, a complete vehicle model with 25 degrees of freedom is established and the dynamic equations of vehicle motion are derived, which is solved through the Newmark-β method. The random vibration phenomenon of the wheel with changes in excitation of track irregularity and stiffness coefficient of elastic layer is simulated. Finally, dynamic numerical calculations are carried out and according to the dynamic calculation results, the following conclusions can be drawn:

1.As the stiffness coefficient of the elastic layer of the wheel increases, the fluctuation coefficient of the vertical acceleration of the wheel shows a spring-back trend; namely it initially decreases gradually, and then increases gradually after reaching a minimum value. The stiffness coefficient corresponding to the minimum value of fluctuation of acceleration is usually the optimal value required for the design.

2.The smaller the stiffness coefficient of the elastic layer, the more readily the maximum value of vertical acceleration of the wheel is affected by the track irregularity. The larger the stiffness coefficient of the elastic later, the greater the minimum value of vertical acceleration of the wheel is affected by track irregularity. Taking the above conclusion as a reference, an appropriate stiffness coefficient of the elastic layer can be selected according to the need for maximum and minimum values in practice.

3.In terms of determining the optimal vertical vibration of the wheel, the lower the degree of track irregularity, the larger the stiffness coefficient of the elastic layer that must be selected.

In conclusion, the selection of an appropriate value of the stiffness coefficient of the elastic wheel damping structure has an important role in reducing wheel vibration. If the elastic stiffness is too small or too large, there is an increase in wheel vibration and this study provides a new method to obtain an appropriate range of stiffness coefficients of elastic layer and verifies the importance of elastic wheel in reducing random vibration of railway system, promoting the improvement of standards of elastic wheel. The proposed model therefore provides new insights on the effect of wheel elasticity on vibration characteristics.

Acknowledgement

References

1. Slatineanu L, Sebeşan I, Arsene S, Manea I, Merticaru V, Mihalache AM, et al. Construction of elastic wheels on light rail vehicles. MATEC Web of Conferences. 2018;178.

2. Naeimi M, Ali Zakeri J, Shadfar M, Esmaeili M. 3D dynamic model of the railway wagon to obtain the wheel-rail forces under track irregularities. Proceedings of the Institution of Mechanical Engineers, Part K: Journal of Multi-body Dynamics. 2015;229(4):357–69.

3. Shi W, Miao L, Luo J, Zhang H. The Influence of the Track Parameters on Vibration Characteristics of Subway Tunnel. Shock and Vibration. 2018;2018:1–12

4. Khajehdezfuly A. Effect of rail pad stiffness on the wheel/rail force intensity in a railway slab track with short-wave irregularity. Proceedings of the Institution of Mechanical Engineers, Part F: Journal of Rail and Rapid Transit. 2019;233(10):1038–49.

5.Zefeng Wen, Lei Wu, Wei Li, Xuesong Jin , Minhao Zhu. Three-dimensional elastic–plastic stress analysis of wheel–rail rolling contact. wEAR 2011; 271:426-436.

6.Xin Zhao, Zili Li. The solution of frictional wheel–rail rolling contact with a 3D transient finite element model Validation and error analysis. Wear 2011; 271: 444-452.

7.Santamaría J, Vadillo EG and Gómez J. A comprehensive method for the elastic calculation of the two-point wheel–rail contact. Vehicle System Dynamics 2006; 44: 240-250.

8. Dinh VN, Kim KD, Warnitchai P. Dynamic analysis of three-dimensional bridge–high-speed train interactions using a wheel–rail contact model. Engineering Structures. 2009;31(12):3090-106.

9. Chopra AK. Dynamics of structures. Upper Saddle River, NJ: Prentice Hall, 1995.

10. Bozzone M, Pennestri E and Salvini P. A lookup tablebased method for wheel–rail contact analysis. Proc IMechE, Part K: J Multi-body Dynamics 2011; 225:127–138.

11. Recuero AM, Escalona JL and Shabana AA. Finite element analysis of unsupported sleepers using threedimensional wheel–rail contact formulation. Proc IMechE, Part K: J Multi-body Dynamics 2011; 225: 153–165.

12. Shabana AA and Rathod C. Geometric coupling in the wheel/rail contact formulations: a comparative study. Proc IMechE, Part K: J Multi-body Dynamics 2007;221: 147–160.

13. Shabana AA, El-Ghandour AI and Zaazaa KE. Study of the effect of the spiral geometry on wheel/rail contact forces. Proc IMechE, Part K: J Multi-body Dynamics 2011; 225: 111–125.

14. Gohar R and Rahnejat H. Fundamentals of tribology. London: World Scientific, 2008.

15. Flores P, Ambro′sio J, Claro JCP, et al. Influence of the contact-impact force model on the dynamic response of multi-body systems. Proc IMechE, Part K: JMulti-body Dynamics 2006; 220: 21–34.

16.Ames WF and Ames W. Nonlinear partial differential equations in engineering. New York: Academic Press, 1972.

17.Greenwood, J.A. and Tripp, J.H., "The contact of two nominally flat rough surfaces", Proceedings of the institution of mechanical engineers, 1970, 185(1), pp. 625-633.

18.Leighton, M., Morris, N., Gore, M., Rahmani, R., Rahnejat, H. and King, P.D., "Boundary interactions of rough non-Gaussian surfaces", Proceedings of the Institution of Mechanical Engineers, Part J: Journal of Engineering Tribology, 2016, 230(11), pp. 1359-1370.

19.Wang Z, Long Z, Li X. Track Irregularity Disturbance Rejection for Maglev Train Based on Online Optimization of PnP Control Architecture. IEEE Access. 2019;7:12610-9.

20.Hwang SH, Kim S, Lee K-C, Jang SY. Effects of Long-Wavelength Track Irregularities Due to Thermal Deformations of Railway Bridge on Dynamic Response of Running Train. Applied Sciences. 2018;8(12).

21.Xu L, Zhai W, Gao J, Meacci M, Chen X. On effects of track random irregularities on random vibrations of vehicle–track interactions. Probabilistic Engineering Mechanics. 2017;50:25-35.

22.Xu L, Zhai W, Gao J. Extended applications of track irregularity probabilistic model and vehicle–slab track

coupled model on dynamics of railway systems. Vehicle System Dynamics. 2017;55(11):1686-706.

23.Ning J, Lin J, Zhang B. Time–frequency processing of track irregularities in high-speed train. Mechanical Systems and Signal Processing. 2016;66-67:339-48.

24.Choi IIY, Um J-H, Lee JS, Choi H-H. The influence of track irregularities on the running behavior of high-speed trains. Proceedings of the Institution of Mechanical Engineers, Part F: Journal of Rail and Rapid Transit. 2012;227(1):94-102.

25. Morton KW. Numerical solution of partial differential equations: an introduction. Cambridge, UK: Cambridge University Press, 2005

26.Wang Z, Long Z, Li X. Track Irregularity Disturbance Rejection for Maglev Train Based on Online Optimization of PnP Control Architecture. IEEE Access. 2019;7:12610-9.

Appendix 1
Notation

g	Gravitational acceleration
M_c M_t M_w M_{tan}	Mass of car, bogie, wheelset, wheel hub
J_{cx} J_{cz} J_{tx} J_{tz} J_{wx}	Car（z,x）, bogie（z,x）and wheelset moment of inertia
K_{s1} K_{s2} K_{s3}	Primary, Secondary, tertiary suspension stiffness
C_{s1} C_{s2} C_{s3}	Primary, Secondary, tertiary suspension damping
l_1, l_2	Primary, Secondary, wheel suspension lengths
$G_{tan\,k}$	The gravity of the wheel
b_1 b_2 b_w	Primary, Secondary, wheel suspension widths
KH	Hertz spring constant
r_r, r_w	Wheel rolling and rail cross section radius
E	Young's modulus elastic ratio
μ	Poisson's ratio
v_c v_t v_w v_{tan}	Displacement of carriage, bogie and wheel
φ_c φ_t φ_w	Rolling motion in z-axis of carriage, bogie and wheel
R_c, R_t, R_w	Rolling motion in x-axis of carriage, bogie and wheel